International Journal of Modern Manufacturing Technologies
ISSN 2067–3604, Vol. XVII, No. 2 / 2025
https://doi.org/ 10.54684/ijmmt.2025.17.2.7

ECO-FRIENDLY SYNTHESIS OF NANO-HYDROXYAPATITE FROM BIOGENIC WASTE VIA MECHANICAL MILLING

Meor Abdullah Ghazey Noor Azman[1], Ismail Zainol[1,2], Charles Christopher Sorrell[3], Che Nor Aiza Jaafar[4], Nurulsaidah Abdul Rahim[1,2], Mustafa Mudzafar[5]

[1]Department of Chemistry, Faculty of Science and Mathematics, Universiti Pendidikan Sultan Idris, UPSI Proton City, 35900 Tanjung Malim, Perak, Malaysia.
[2]Nanotechnology Research Centre, Faculty of Science and Mathematics, Universiti Pendidikan Sultan Idris, UPSI Proton City, 35900 Tanjung Malim, Perak, Malaysia.
[3]School of Materials Science and Engineering, Hilmer Building, University New South Wales, Sydney, New South Wales, 2052, Australia
[4]Department of Mechanical and Manufacturing Engineering, Faculty of Engineering, Universiti Putra Malaysia, 43000 Serdang, Selangor, Malaysia.
[5]Department of Medical Physics, Faculty of Medical Applied Sciences, University of Kerbala, 56001 Karbala, Iraq

Corresponding author: Ismail Zainol, ismail.zainol@fsmt.upsi.edu.my

Abstract: The growing demand for sustainable and environmentally friendly materials has spurred interest in green synthesis approaches for bioactive compounds. In this study, nano-hydroxyapatite (nHA) was synthesized from fish scale biowaste via a top-down mechanical milling method. Fish scales, a renewable and calcium/phosphate-rich waste product, were first calcined to produce FsHA and then subjected to ball milling to produce nanoscale FsHA particles. The resulting material was characterized using particle size analysis, X-ray diffraction (XRD), Fourier transform infrared spectroscopy (FTIR), scanning electron microscopy (SEM), and transmission electron microscopy (TEM). FTIR analysis on ball-milled FsHA revealed the presence of HA peaks together with carbonate absorption bands, confirming the presence of B-type carbonate substitutions, indicating partial replacement of phosphate groups by carbonate ions. The presence of C-H groups indicates the potential for polyethylene (PE) contamination originating from the milling container. XRD analysis revealed a pronounced reduction in crystallinity and peak intensity, consistent with a reduction in crystallite size, lattice distortion, and partial amorphization induced by mechanical stress and carbonate incorporation. TEM and STEM imaging verified particle sizes in the 20–200 nm range but also revealed severe agglomeration and the presence of nanoplastic debris (4–5 nm), generated by abrasion of the PE container during milling. These results highlight the dual influence of milling conditions and container material on the purity, stability, and dispersion of biogenic nHA, emphasizing the importance of careful material selection in preventing unwanted contamination and preserving functionality for biomedical applications.
Key words: mechanical milling, fish scale hydroxyapatite; nano hydroxyapatite, biogenic materials

1. INTRODUCTION

Hydroxyapatite (HA), chemically represented as $Ca_{10}(PO_4)_6(OH)_2$, is a calcium phosphate ceramic extensively studied for its outstanding biocompatibility, bioactivity, and structural similarity to human bone and dental enamel. In recent years, nano-sized hydroxyapatite (nHA) has gained considerable attention across various fields, including bone tissue engineering [1], orthopaedics [2], dentistry [3], and nutritional supplements [4], due to its enhanced surface area, superior bioresorption, and improved integration with biological tissues compared to bulk HA. Traditional HA synthesis methods, such as wet chemical precipitation [5], sol-gel [6], hydrothermal processing [7], solid-state reactions [8], and microwave-assisted [9], often require harsh reaction conditions, toxic reagents, or high energy input, limiting their environmental sustainability and economic feasibility. To address these challenges, biowaste-derived hydroxyapatite has emerged as a promising and sustainable alternative. Fish scales, a plentiful byproduct of the seafood industry, provide a rich natural source of calcium and phosphate suitable for HA extraction [10,11]. Utilizing fish scales not only valorizes waste materials but also mitigates environmental pollution concerns. Although prior research has successfully extracted HA from natural sources like bovine bones, eggshells, and fish bones, fish scales remain relatively underexploited despite their high mineral and organic content [12].

Previous studies have demonstrated the feasibility of synthesizing HA from fish scales using chemical methods. For example, Dep et al. (2019) employed calcination followed by chemical precipitation to extract HA from *Labeo rohita* scales, while Kumar et al. (2016) used wet chemical synthesis to obtain crystalline HA from catla fish scales, albeit with considerable chemical use and energy consumption [13,14]. Recent advancements such as microwave-assisted and enzyme-mediated extraction methods, like those by Burdusel et al. (2016), [15]. However, these methods often involve multi-step processing, chemical waste, and thermal treatment. Zainol et al. have extracted HA from Tilapia fish scales using thermal [16] and chemical method [17]. Despite extensive research on fish scale-derived HA extraction, the fabrication of nano-sized HA from these sources using purely mechanical methods remains largely unexplored. Mechanical milling, a solvent-free, surfactant-free process, is well-established in material science for particle size reduction, homogenization, and inducing mechanochemical transformations, aligning well with green chemistry principles. While mechanical milling has been successfully applied to produce nanomaterials from other biogenic sources such as oyster shells, its application to fish scale-derived HA has not been comprehensively studied [18].

This study aims to bridge this gap by developing a simple, cost-effective, and eco-friendly mechanical milling process to synthesize nano-hydroxyapatite from fish scales. The synthesized nHA will be characterized using XRD, FTIR, TEM, and other analytical techniques to evaluate its structural, morphological, and compositional properties. By comparing these results with conventional chemical synthesis approaches, this work seeks to demonstrate the potential of mechanical milling as a sustainable technology for converting biowaste into high-value nanomaterials suitable for biomedical applications. In summary, although various techniques exist for producing HA from natural sources, this research introduces a novel, green, and sustainable route combining fish scale utilization and mechanical milling. This approach supports the principles of circular economy and sustainable materials science by converting biowaste into valuable nanomaterials with reduced environmental impact.

2. MATERIALS AND METHODS

2.1. Materials

Tilapia fish scales were collected from the Tanjung Malim market in Perak, Malaysia, thoroughly rinsed to remove dirt, and immersed in 0.2 M hydrochloric acid to eliminate fats and residual impurities. After several washes with distilled water, the scales were oven-dried at 80 °C. The dried material was then calcined in a furnace at 1000 °C for 2 h to produce fish ash. The ash was milled using a wet milling machine (Poul O. Abbe, USA) for 48 h and subsequently oven-dried to obtain fish scale–derived hydroxyapatite (FsHA) powder. The FsHA powder was further milled for different durations, and the resulting FsHAp particles were characterised for their nanoparticle properties.

2.2. Mechanical milling of FsHA

The FsHA underwent another series of wet ball milling (Poul O. Abbe, USA) process for 96 to 240 hours to generate a homogenized FsHA slurry, which was subsequently freeze-dried to yield fine FsHA powder. The sample coding and milling time are shown in Table 1.

Table 1. Milling time and sample coding

No	Milling Time (hour)	Coding
1	0	HA1
2	96	HA2
3	140	HA3
4	240	HA4

2.2. Characterisation of nano HA particles

Particle size distribution was measured using a Malvern Zetasizer Nano ZS based on Dynamic Light Scattering (DLS)**.** Samples were dispersed in deionized water and filtered through a 0.22 µm syringe filter to remove dust and aggregates. Measurements were conducted at 25 °C using a disposable polystyrene cuvette**,** with a backscatter detection angle of 173°**.** The refractive index and viscosity of the dispersant were input into the software, and each sample was equilibrated for 2 minutes before measurement. Results are reported as Z-average hydrodynamic diameter and polydispersity index (PDI)**,** averaged over three runs per sample.

Fourier-transform infrared (FTIR) spectroscopy was performed to characterize functional groups in the fish scale–derived nano hydroxyapatite (nFsHA) and FsHA. Before analysis, the powders were oven-dried at 80–100 °C for

2 h to remove surface moisture and CO_2. For measurements, samples were analyzed using an [FTIR instrument model] equipped with a [diamond ATR accessory / KBr pellet setup]. Spectra were collected in the range of 4000–400 cm^{-1} at a resolution of 4 cm^{-1} with 32–64 scans co-added for each spectrum. The crystalline structure of the synthesized samples was analyzed using X-ray diffraction (XRD) with a Rigaku MiniFlex diffractometer equipped with Cu-Kα radiation (λ = 1.5406 Å**)**, operating at 40 kV and 30 mA. Data were collected over a 2θ range of 10° to 80° with a step size of 0.02° and a scanning speed of 1°/min. Phase identification was performed by comparing the diffraction patterns with standard reference data from the JCPDS database**.**
The morphology and particle size of nFsHA were analyzed using a field emission scanning electron microscope (FESEM) (Hitachi SU8020) and a transmission electron microscope (TEM) (JEOL JEM-2100) attached with energy-dispersive x-ray spectroscopy (EDX) for elemental analysis. A small amount of nHA powder was dispersed in ethanol via ultrasonication for 10 minutes, and a drop of the suspension was deposited onto a carbon-coated copper grid. The grid was air-dried before imaging. FESEM was run under STEM mode, whereas TEM analysis was performed at an accelerating voltage of 200 kV, and images were captured to evaluate particle shape, size, and dispersion.

3. RESULTS AND DISCUSSION

3.1. Particle size analysis

Dynamic light scattering (DLS) analysis demonstrated a significant reduction in the hydrodynamic particle size of FsHA as milling time increased. The DLS analysis results for FsHA and FsHA milling at different times, 96, 140, and 240 hours, are shown in Figure 1, and the z-average diameter and PDI results were summarised in Table 2. The results show a single peak for most of the samples, indicating monodisperse particles. Intensity in the plot represents the amount of light scattered by particles in the sample at each particle size, but it does not directly represent the number of particles.
The starting FsHA used had an average particle size around 3232 nm and reduced to 2,278 nm after milling for 96 hours with a polydispersity index (PDI) of 0.316 (Figure 1b). These results indicate a broad size distribution dominated by large aggregates. Shorter milling durations resulted in micron-sized HA with high PDI values due to incomplete fragmentation and persistent agglomeration tendencies [19] facilitated by van der Waals and hydrogen bonding interactions [20].

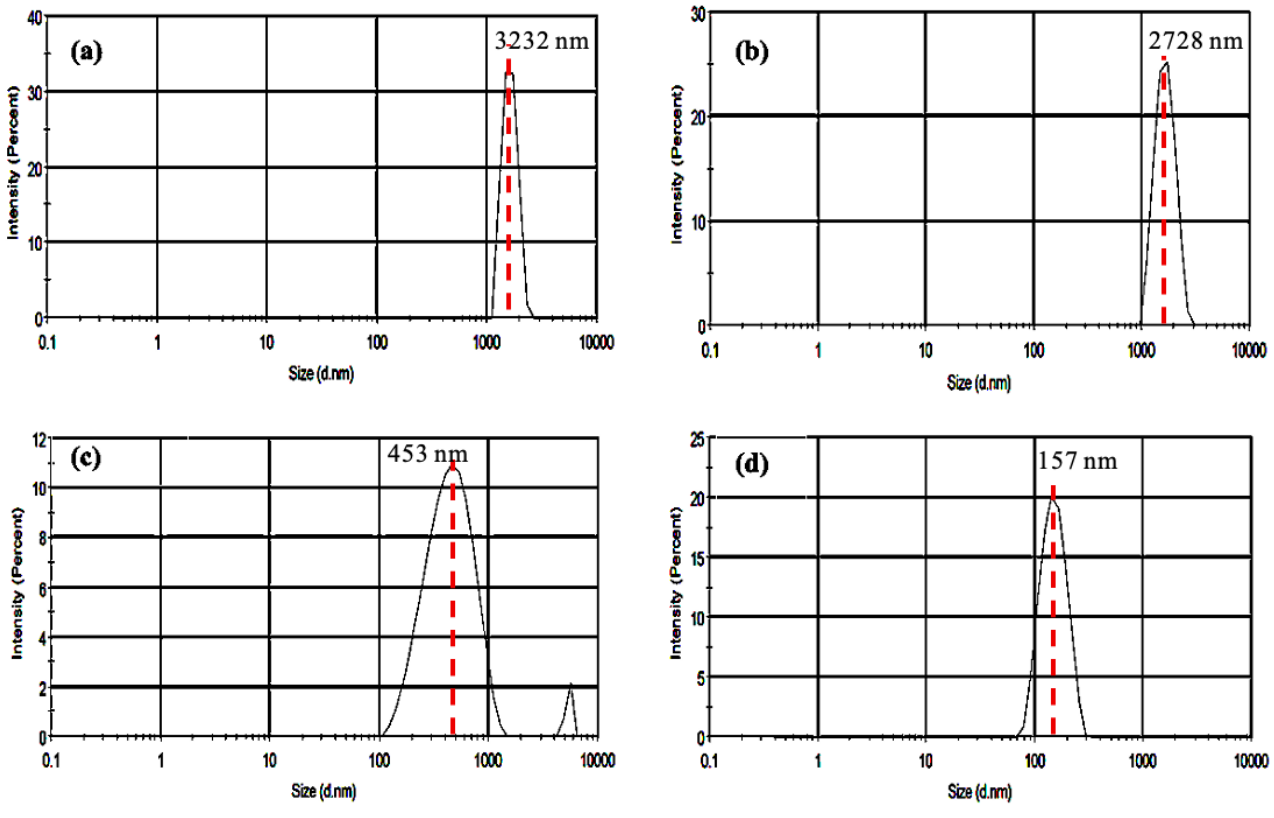

Fig.1. DLS analysis results for FsHA samples milling at different times (a) 0 hours, (b) 96 hours, (c) 140 hours, and (d) 240 hours.

Extending the milling time to 140 hours significantly reduced the average particle size to 453 nm, but the PDI number is still high, around 0.354 (Figure 1c), reflecting incomplete fragmentation of nanoparticles and nanoscale dimensions were not yet achieved, suggesting that further milling was necessary. Prolonging the milling duration to 240 hours further decreased the average size to 157 nm and reduced the PDI to 0.233 (Figure 1d), demonstrating enhanced particle uniformity and stability. This aligns with previous studies showing that extended milling promotes effective deagglomeration and size reduction, producing nanosized FsHA (nFsHA) particles suitable for biomedical applications [21].

Table 2. Milling time and sample coding

Sample	Milling Time (hours)	Peak intensity (Z-Average Diameter, nm)	PDI
HA1	0	3232	0.459
HA2	96	2278	0.316
HA3	140	453	0.354
HA4	240	157	0.233

Longer milling increased the frequency of collisions between zirconia balls and FsHA particles, promoting deagglomeration and fragmentation of primary particles, thereby yielding nanosized FsHA with improved uniformity. A PDI below 0.3 at 240 hours indicates a relatively monodisperse system, which is desirable for biomedical applications where stability and reproducibility are critical. The reduction in particle size also increases surface area, potentially enhancing bioactivity and interactions with polymer matrices or biological tissues.

3.2. FTIR Analysis

Fourier transform infrared (FTIR) spectroscopy was employed to confirm the chemical structure and assess the purity of nFsHA after ball milling. The FTIR spectrum of raw FsHA (Figure 2(a)) and milled FsHA (Figures 2b-2c) exhibited the characteristic vibrational modes of the phosphate group (PO_4^{3-}) typical of standard hydroxyapatite [22]. A strong and sharp peak at 961 cm^{-1} was assigned to the ν_1 symmetric stretching mode of PO_4^{3-}, while the broad band between 1000–1020 cm^{-1} corresponded to the ν_3 asymmetric stretching vibration. The presence of a distinct doublet at 598 and 554 cm^{-1}, attributed to the ν_4 bending mode of PO_4^{3-}, confirmed the apatite crystalline structure [13]. The hydroxyl (OH^-) stretching vibration appeared as a narrow band at 3571 cm^{-1}, accompanied by the OH vibration mode at 630 cm^{-1}, indicating that the hydroxyl channels in the HA lattice remained intact after mechanical processing [23].

In addition to the phosphate and hydroxyl groups, weak but discernible bands were observed at 1422 cm^{-1} and 872 cm^{-1} for sample milling for 96 to 240 hours (Figure 2b to 2c) corresponding to the ν_3 and ν_2 modes of the carbonate (CO_3^{2-}) ion, respectively. These signals indicate B-type carbonate substitution, where carbonate replaces phosphate sites, a common feature in biologically derived apatite such as fish-scale HA [24]. The carbonate incorporation is known to increase lattice disorder and enhance the biological resorption rate, which may be advantageous for biomedical applications [23].

There is no absorptions at appeared at ~1650 cm^{-1} (amide I), ~1540 cm^{-1} (amide II), and weak aliphatic C–H stretching bands at ~2920 and ~2850 cm^{-1} which indicating no residual of organic matter, likely collagen fragments, from the fish scales. Such residuals are typical in biogenic HA, but due to high calcination temperature > 1000 °C, these fragment was completely removed from fish scales [25]. The preservation of both PO_4^{3-} and OH^- vibrational modes, along with the observed carbonate substitution, confirms that the product retained its apatite structure after ball milling. The slight shifting of phosphate bands compared to the original FsHA was reported in literature [14], suggesting a slight change in crystallinity, consistent with the particle size refinement into the nanometer range and possible lattice strain induced by high-energy milling.

A distinct absorption band at approximately 2917 cm^{-1} appeared in the FTIR spectra of samples milled for 140 to 240 hours (Figure 2c and 2d). This band corresponds to CH_2 asymmetric stretching vibrations, which are characteristic of hydrocarbon-based polymers such as polyethylene (PE) [26]. The observation indicates that the PE container surface was abraded during prolonged milling by the hard surface of FsHA, which exhibits abrasive properties. These results highlight the critical importance of selecting appropriate container materials for extended milling processes to minimize contamination that could compromise the integrity of the milled products in subsequent applications. The presence of nanoplastic particles will be further verified through TEM analysis.

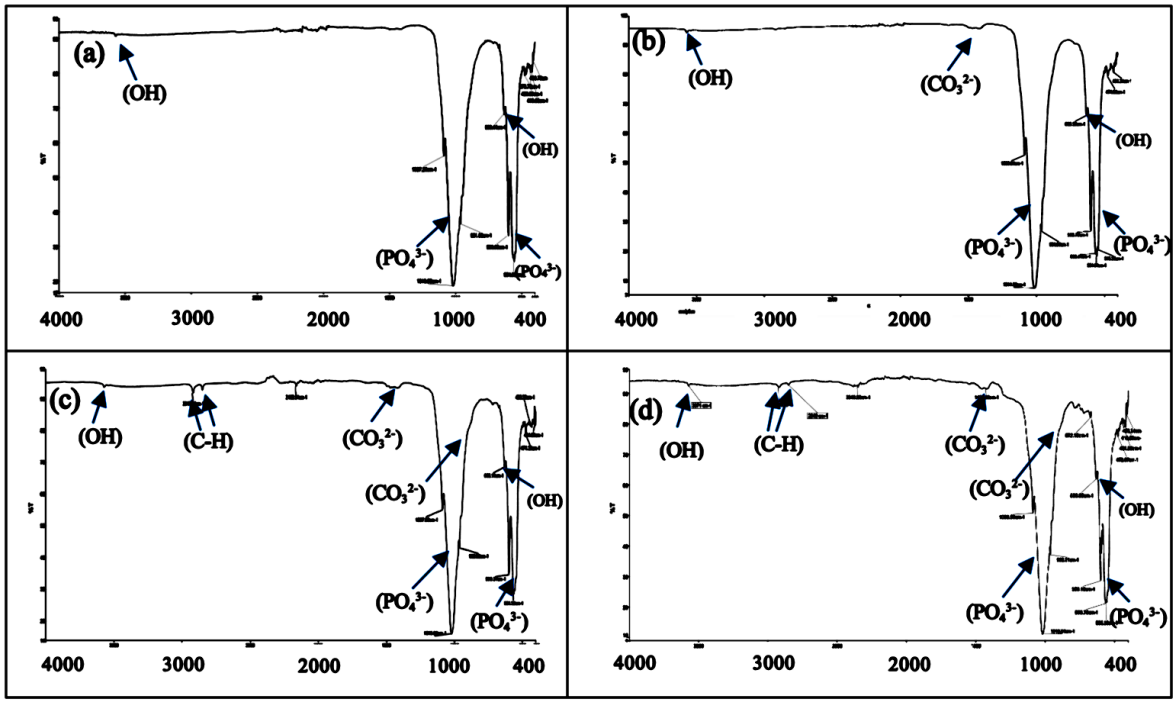

Fig. 2. Fourier transform infrared (FTIR) spectrum after ball milling (a) 0 hours, (b) 96 hours, (c) 140 hours, and (d) 240 hours.

3.3. XRD Analysis

X-ray diffraction (XRD) patterns of biogenic hydroxyapatite (HA) typically exhibit sharp peaks characteristic of high crystallinity and nanostructured domain of biologically derived HA as shown in Figure 3. The major diffraction peaks correspond to the hexagonal crystal system with characteristic reflections observed at $2\theta \approx 25.9°$ (002), 31.8° (211), 32.9° (112), 34.0° (300), and 39.8° (310) (JCPDS card No. 09-0432) [27]. In biogenic HA, the broad and merged peak around 31–33° 2θ is particularly prominent and often includes overlapping contributions from the (211), (112), and (300) planes. The additional or intensified peak near 32° 2θ is commonly attributed to the presence of B-type carbonate substitution, where CO_3^{2-} ions replace PO_4^{3-} groups in the HA lattice [28]. This substitution leads to lattice distortion, peak shifting, and broadening, reflecting reduced crystallinity and increased biological resemblance. Furthermore, in biogenic samples, minor secondary phases such as beta-tricalcium phosphate (βTCP) appear at 31.2° 2θ may contribute to additional or asymmetrical peaks near this region.

The observed reduction in XRD peak intensity of fish-derived hydroxyapatite (HA) after prolonged ball milling is primarily attributed to a decrease in crystallinity and crystallite size**,** along with increased lattice strain and defect density induced by mechanical processing. Ball milling introduces high-energy collisions that disrupt the long-range order of the HA crystal lattice, leading to partial amorphization and the formation of nanocrystalline domains**.** As a result, XRD peaks become broader and less intense**,** reflecting a less ordered structure [29]. In biogenic HA, this effect is further amplified due to the presence of carbonate substitution**,** residual organic matter, and minor phases (such as β-TCP), which are more sensitive to mechanical stress. These structural changes reduce the ability of the crystal planes to coherently diffract X-rays, thus lowering peak intensity. Additionally, surface contamination from the milling media (e.g., polyethylene) may contribute to background noise, further diminishing peak sharpness and clarity.

3.4. Morphology analysis

SEM analysis in transmission mode (STEM) was performed to observe the nanostructure of FsHA, as shown in Figure 4(a). The ball-milled hydroxyapatite (HA) nanoparticles exhibited irregular and non-uniform morphology, as observed in the STEM image. The particles showed a wide size distribution ranging from 20 to 200 nm, which is consistent with the mechanical fragmentation mechanism of ball milling. During milling, impact and shear forces cause random particle breakage, producing angular and unevenly shaped particles. In addition, nanoparticle agglomeration occurred due to high surface energy, contributing to the presence of larger clusters in the micrographs. TEM micrographs further showed that, although the hydroxyapatite (HA) particles remained within the nanometer range after ball milling, a

significant degree of agglomeration was present, with many particles trapped or clustered between thin layers. This phenomenon can be attributed to the high surface energy and reactivity of nHA particles, which drive agglomeration as a thermodynamically favourable process to reduce surface area [30].

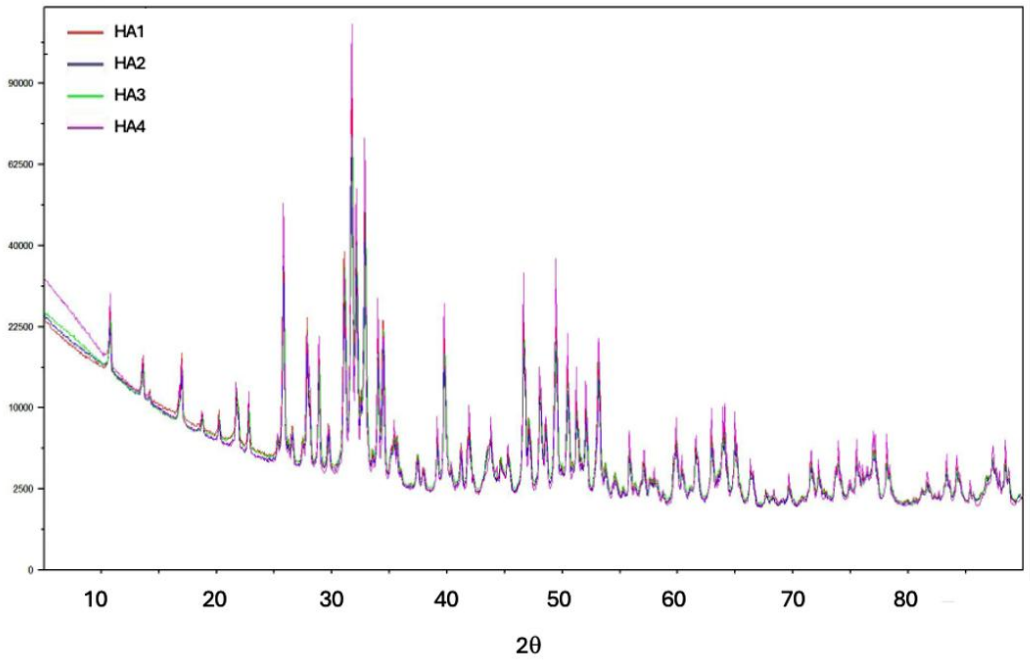

Fig. 3. Overlaid X-ray diffraction (XRD) patterns of HA1, HA2, HA3, and HA4.

From Figure 4(a), closed examination revealed the fragment of nanoparticles with a diameter of 4–5 nm surrounding HA particles. EDX analysis was carried out and found that the particles are characteristic of polyethylene (PE). Prolonged mechanical milling of materials in PE containers may have abraded the polymer surface, generating PE nanoparticles that became intermixed with or adsorbed onto the HA particles. The nanoscale HA particles can readily adhere to such polymeric surfaces through electrostatic interactions, van der Waals forces, or hydrophobic interactions, particularly in the absence of surfactants or dispersants. Furthermore, electrostatic charge accumulation during milling may contribute to particle embedding within PE layers. These interactions not only enhance agglomeration but may also alter the surface chemistry of HA, as indicated by the C–H stretching bands observed in FTIR. Collectively, these findings underscore the critical role of container material and milling conditions in determining nanoparticle stability and dispersion behavior.

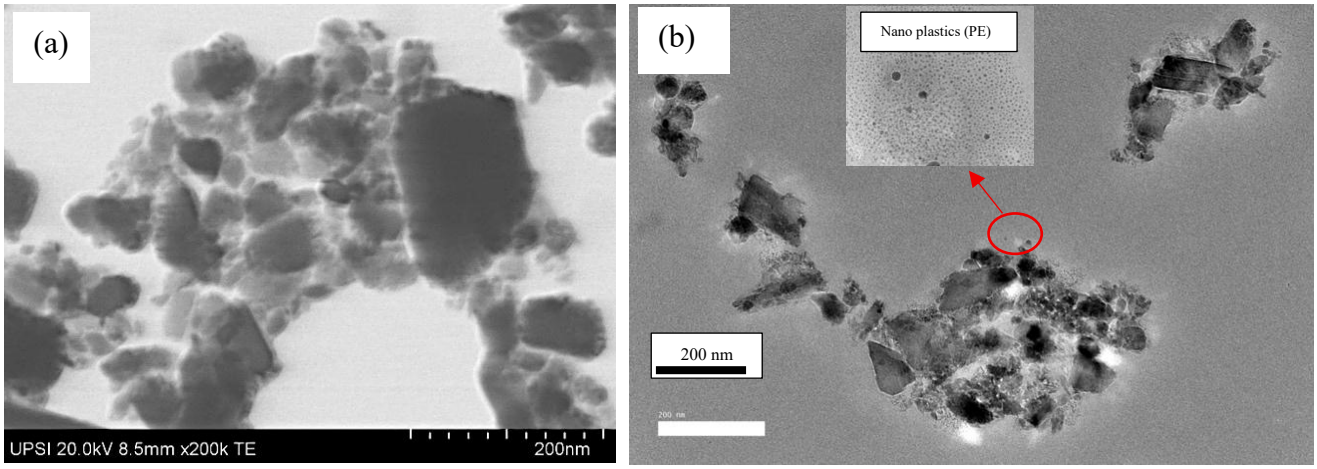

Fig. 4. (a) Scanning electron micrograph in transmission mode (STEM) and (b) transmission electron micrograph (TEM) (insert is a zoom of nano plastic, PE particles with a diameter of 4 to 5 nanometers)

4. CONCLUSIONS

Structural and morphological analyses of nano-hydroxyapatite (nHA) derived from fish scales and subjected to prolonged ball milling in polyethylene (PE) containers revealed notable physicochemical modifications. FTIR spectroscopy confirmed B-type carbonate substitution within the HA lattice, along with C–H stretching bands arising from PE contamination. XRD patterns showed reduced crystallinity and peak intensity, consistent with crystallite size reduction, lattice distortion, and partial amorphization induced by high-energy milling and carbonate incorporation. TEM imaging verified the nanoscale dimensions of nFsHA particles (20–200 nm after 240 h of milling) while also indicating significant nanoplastic contamination, likely originating from mechanical abrasion of the PE container by the hard FsHA particles. These findings demonstrate the combined influence of milling conditions and container material on the structural integrity, purity, and dispersion of biogenic nFsHA, underscoring the importance of selecting appropriate milling containers to ensure material quality for future applications.

Author contributions: The contributions of the authors can refer to the following stages of a paper accomplishment: conceptualization was contributed by Zainol, I. (Zainol I). Conception or design of the paper, data analysis was done by I. Zainol; data acquisition and analysis were done by Meor Abdullah Ghazey Noor Azman; methodology development was carried out by Che Nor Aiza Jaafar and Mustafa; supervision, validation of data and editing was conducted by Prof Chris Sorrell, I. Zainol and Nurul Saidah. All authors have read and agreed to the published version of the manuscript.

Funding source: This research was supported by the Ministry of Higher Education (MoHE) through the FRGS research grant 2023-0088-103-02 (FRGS/1/2023/STG05/UPSI/01/1).

Conflicts of interest: There is no conflict of interest.

Acknowledgements: This research was supported by the Ministry of Higher Education (MOHE), Malaysia, through the Fundamental Research Grant Scheme 2023-0088-103-02 (FRGS/1/2023/STG05/UPSI/01/1). The authors would like to thank Jerry from the Materials Science Centre, UNSW, and Mr. Zulkifly from UKM for helping to analyze the sample using XRD and Zeta Sizer.

5. REFERENCES

[1]. Xiuqiong C., Jiayi L., Yanan B., Ting W., Jiji F., Huiqiong Y., Qiang L., (2025), *Dodecyl glycoside intercalated organo-montmorillonite promoted biomimetic alginate/microcrystalline cellulose/nano-hydroxyapatite composite hydrogels for bone tissue engineering*, International Journal of Biological Macromolecules, 310, pp. 143304.

[2]. Mangal R., Amit B., Susmita B., (2011), *Induction plasma sprayed nano hydroxyapatite coatings on titanium for orthopaedic and dental implants,* Surface & Coatings Technology, 205, 2785–2792.

[3]. Abdulrazzaq H., Hiba H. D., Lama A., *Preparation of nano hydroxyapatite loaded with syrian inula extract against dental caries*, Materials Chemistry and Physics, 327, pp. 129872.

[4]. Jared J. S., Yuqiang B., Justin K., Pierre H., Kiril H., Paul W., (2017), *Detection and dissolution of needle-like hydroxyapatite nanomaterials in infant formula*, NanoImpact, 5, 22–28.

[5] Azade Y., Suat Y. (2018). Wet chemical precipitation synthesis of hydroxyapatite (HA)powders, *Ceramics International*, 44(8), 9703-9710.

[6] Kim, I.S.; Kumta, P.N. *Sol–gel synthesis and characterization of nanostructured hydroxyapatite powder.* Mater. Sci. Eng. B 2004, 111, 232–236.

[7]. Chang C. Y., Pin Y. L., Gobinda D., Jyoti P. M., Raju K. S., Chin W. W., Shafiqa A., Chien Y. C. (2025). *Hydrothermal synthesis of hydroxyapatite nanoparticles using biosurfactant and application on mesenchymal stem cells,* Ceramics International, 51(14), 19091-19101.

[8]. Mashrafi M., Nigar S. P., Fariha C., Sahadat H., Monika M., Saiful Q., Shirin A. J., Samina A. (2025). Environmental remediation by Materials Today: Proceedings 16, 1942-1948 Solid state synthesis utilizing waste chicken eggshell and adsorption experiment with Congo red dye. Journal of Saudi Chemical Society, 27(5), pp. 101690

[9] Deni F. F., Rilo C. M, Yustina M. P., Rifky I., Jamari J., Athanasius P. B. (2025). *Microwave-assisted synthesis of nanocrystalline hydroxyapatite using calcium supplies from green mussel shells with synthesis time optimization*. Nano-Structures & Nano-Objects, 42, pp. 101484

[10] Zainol I., Adenan N. H., Rahim N. A and Jaafar C. N. A. (2019). *Extraction of natural* hydroxyapatite *from tilapia* fish scales *using alkaline treatment,* Materials Today: Proceedings 16, 1942–1948.

[11] Patwary M. A., Yasin M., Azam M. S. and Hossain M. A. (2025), *Extraction and industrial valorization of collagen, gelatin, and hydroxyapatite from freshwater fish scales: A review.* Food and Bioproducts Processing, 154, 319-333

[12]. Akshita S., Nachiket K., Kannan N., Subbalaxmi S., (2021), *Review on the extraction of calcium supplements from eggshells to combat waste generation and chronic calcium deficiency*, Environmental Science and Pollution Research, 28, 46985–46998.
[13] Payel D., Emon B., Sumit D. L., Aishah B. D., (2019), *Synthesis of hydroxyapatite from Labeo rohita fish scale for biomedical application*, Materials Today Proceedings, 15, 277-283.
[14] Kumar G. S., Sivakumar T., Karthi S., Govindan R., Girija E. K., (2016), *Fish Scale Derived Nanocrystalline Hydroxyapatite: A Potential Candidate for Orthopedic Applications*, Journal of Bionanoscience, 10(2), 140-144.
[15] Alexandra C. B., Ionela A. N., Alexandra C. B., Cristina C., Alexandru M. G., Alina M. H., Carmen C., Lia M. D., Miruna S., Ecaterina Andronescu, (2023), *Microwave-Assisted Hydrothermal Treatment of Multifunctional Substituted Hydroxyapatite with Prospective Applications in Bone Regeneration*, Journal Functional Biomaterial, 14(7), pp. 378.
[16] Zainol, I., Alhussein, A. M., Jaafar, C.N.A., Mustafa, M. (2025). *Epoxy composites reinforced with fish-derived hydroxyapatite for load-bearing biomedical applications*, Malaysian Journal of Microscopy, 21(1), 91-10.
[17]. I Zainol, NH Adenan, NA Rahim, CNA Jaafar. (2019). *Extraction of natural hydroxyapatite from tilapia fish scales using alkaline treatment.* Materials Today: Proceedings, 16, 1942-1948.
[18] Thakur P. Y., Ram M. Y., Dinesh P. S., (2012). *Mechanical Milling: a Top Down Approach for the Synthesis of Nanomaterials and Nanocomposites,* Nanoscience and Nanotechnology, 2(3), 22-48.
[19] Maria A. G., Aniek S. B., Maria L. A. D. L., Fedik A. R., Chrismawan A., Junaidi K., (2022), *Fabrication and Characterization of Submicron-Scale Bovine Hydroxyapatite: A Top-Down Approach for a Natural Biomaterial*. Materials, 15, pp. 2324.
[20] Lea A., Lucas S. J., Merel J. W., Adjobo H., Fang Y., Rong W., Sander C. G. L., (2024), *Effect of Hydroxyapatite Nanoparticle Crystallinity and Colloidal Stability on Cytotoxicity*, ACS Biomater Sci Eng. 10(11), 6964–6973.
[21] Sharifah A. S. A. B., Iis S., Mohd H. A. S., (2011), *Mechanochemical Synthesis of Hydroxyapatite Nanopowder: Effects of Rotation Speed and Milling Time on Powder Properties*. Applied Mechanics and Materials, 110-116, 3639-3644.
[22] Abifarin J. K., Obada D.O., Dauda E. T., Dodoo-Arhin D., (2019), *Experimental data on the characterization of hydroxyapatite synthesized from biowastes*, Data Brief, 26, pp. 104485.
[23] LeGeros, R.Z. (2002). *Properties of osteoconductive biomaterials: Calcium phosphates*. Clinical *Orthopaedics and Related Research*, 395, 81–98.
[24] Honey M., Barbara P., Mary M.J. T., (2017), *Carbonate substitution in the mineral component of bone: Discriminating the structural changes, simultaneously imposed by carbonate in A and B sites of apatite,* Journal of Solid State Chemistry, 255, 27–35.
[25] Ismail Zainol, N. H. Adenan, Nurul Saidah, CN Aiza Jaafar, (2019). *Extraction of natural hydroxyapatite from tilapia fish scales using alkaline treatment,* Materials Today Proceedings 16, 1942-1948
[26] Jaafar C. N. A., Zainol. I., Khairani M. I. I., Dele-Afolabi, T. T., (2022). *Physical and Mechanical Properties of Tilapia Scale Hydroxyapatite-Filled High-Density Polyethylene Composites*, Polymers, 14*(2)*, pp. 251.
[27] Kamonwannasit, S., Futalan, C.M., 2020, Khemthong, P. *Synthesis of copper-silver doped hydroxyapatite via ultrasonic coupled sol-gel techniques: structural and antibacterial studies*. J Sol-Gel Sci Technol, 96, 452–463.
[28] Nazia B., Suzi S. J., Hatijah B., Sharifah A., Dagaci M, Z. (2019). *XRD and FTIR study of A&B type carbonatedhydroxyapatite extracted from bovine bone*, AIP Conference Proceedings, 2068, pp. 020100,
[29] Leonel E. C., Nassar E. J., Ciuffi, K. J. Reis, P. S M. J. dos. *Calef (2014). Effect of high-energy ball milling in the structural and textural properties of kaolinite,* Cerâmica, pp. 267-272.
[30] Karin H Müller, Michael Motskin, Alistair J Philpott, Alexander F Routh, Catherine M Shanahan, Melinda J Duer, Jeremy N Skepper (2014). *The effect of particle agglomeration on the formation of a surface-connected compartment induced by hydroxyapatite nanoparticles in human monocyte-derived macrophages*, Biomaterials, 35(3), 1074–1088.

Received: May 15th, 2025 / Accepted: November 18th, 2025 / Paper available online: December 20th, 2025
© International Journal of Modern Manufacturing Technologies.